



# Low-Temperature Sintering Properties of Bi<sub>2</sub>O<sub>3</sub> Doped PZT-5H Piezoelectric Ceramics

Wanzi Mao<sup>1,2</sup> · Qing Xu<sup>1</sup> · Duanping Huang<sup>1,2</sup> · Huajun Sun<sup>1,2</sup> · Feng Zhang<sup>1</sup> · Xiaobin Xie<sup>1</sup>

Received: 18 October 2022 / Accepted: 15 February 2023 / Published online: 3 March 2023  
© The Minerals, Metals & Materials Society 2023

## Abstract

Due to its excellent piezoelectric characteristics and Curie temperatures, PZT-5H piezoelectric ceramics are perfect for creating low-temperature co-fired multilayer devices. The effects of Bi<sub>2</sub>O<sub>3</sub> doping on the low-temperature sintering properties of PZT-5H ceramic powder were investigated in this work. When the mass fraction of Bi<sub>2</sub>O<sub>3</sub> is 0.9%, PZT-5H ceramics can be completely sintered at 850°C. In addition, the chemical composition exhibits the best electrical properties at this doping level and lies at the morphological phase boundary (MPB). The property is as follows:  $d_{33} = 504\text{pC/N}$ ,  $\tan \delta = 0.0296$ ,  $k_p = 0.653$ ,  $Q_m = 30.983$ , and  $T_c = 230^\circ\text{C}$ . A multilayer piezoelectric ceramic actuator was created in this work to better demonstrate the real-world applications of using this material in low-temperature co-fired devices. The multilayer piezoelectric actuator's characterization revealed that the material was tightly attached to the Ag electrode, and that there was minimal Ag diffusion at the bond, with satisfactory co-firing matching. At a drive voltage of 600 V, the multilayer actuator produced a displacement of 2.18  $\mu\text{m}$  and a strain value of 0.109%. This showed that it was feasible to create multilayer piezoelectric ceramic actuators with this material, and that it provides a new alternative material for creating other multilayer piezoelectric ceramic devices.

**Keywords** PZT-5H · Bi<sub>2</sub>O<sub>3</sub> · low-temperature sintering · piezoelectric ceramics actuators

## Introduction

Due to the widespread application of piezoelectric actuators and transformers in recent years, low-temperature sintering piezoelectric ceramic materials have garnered much research interest.<sup>1–4</sup>

High piezoelectric constants and electromechanical coupling coefficients are often needed for the performance of piezoelectric materials to meet the needs of piezoelectric actuators.<sup>5</sup> PZT-5H piezoelectric ceramics have high piezoelectric constants and high stability, and can be used to prepare multilayer piezoelectric ceramic components, which have broad application prospects and are of great interest to researchers.<sup>6</sup> However, PZT-based piezoelectric ceramics

are usually sintered at temperatures above 1200°C. The Pb component in PZT ceramics may be severely volatilized due to high temperatures while sintering.<sup>7</sup> For multilayer piezoelectric ceramic actuators, high melting point Ag-Pd precious metals are currently preferred as inner electrodes. It would cost too much to use such an expensive metal as the inner electrode of the brake.<sup>8</sup> If PZT-based piezoelectric ceramics can be sintered below 900°C, silver can be used as the inner electrode, which will reduce costs and prevent lead oxide volatilization.<sup>9,10</sup>

The most popular and practical method for sintering piezoelectric ceramics at low temperatures is to add sintering aids.<sup>11</sup> The research hotspots of low-temperature sintering additives mainly include low melting point glass materials and low melting point compounds, among which the most common sintering aids include oxides and carbonates, such as ZnO, V<sub>2</sub>O<sub>5</sub>, Li<sub>2</sub>CO<sub>3</sub>, B<sub>2</sub>O<sub>3</sub>, and PbO.<sup>12–14</sup>

It has been reported that many researchers have used LiBiO<sub>2</sub> to fabricate PZT-based piezoelectric ceramic materials with low sintering temperatures and outstanding electrical properties. Yi et al.<sup>15</sup> used LiBiO<sub>2</sub> as a sintering aid to reduce the sintering temperature of 0.35Pb(Ni<sub>1/3</sub>Nb<sub>2/3</sub>)O<sub>3</sub>–0.65Pb(Zr<sub>0.41</sub>Ti<sub>0.59</sub>)O<sub>3</sub> (PNN–PZT)

✉ Duanping Huang  
duanpinghuang@sina.com

<sup>1</sup> School of Materials Science and Engineering,  
Wuhan University of Technology, Wuhan 430070,  
People's Republic of China

<sup>2</sup> Advanced Ceramics Institute of Zibo New &  
High-Tech Industrial Development Zone, Zibo 255000,  
People's Republic of China

ceramics. The ferroelectric and piezoelectric properties of PNN–PZT ceramics were not significantly deteriorated by adding a small amount of LiBiO<sub>2</sub> ( $d_{33} = 538$  pC/N,  $Q_m = 61$ ,  $k_p = 0.62$ , and  $\epsilon_r = 3381$ ). Hong et al.<sup>16</sup> successfully lowered the sintering temperature to 900°C by adding LiBiO<sub>2</sub> to 0.69Pb(Zr<sub>0.47</sub>Ti<sub>0.53</sub>)–0.31Pb[(Zn<sub>0.4</sub>Ni<sub>0.6</sub>)<sub>1/3</sub>Nb<sub>2/3</sub>] (PZT–PZNN) and obtained excellent piezoelectric properties ( $d_{33} = 602$  pC/N,  $k_p = 0.663$ ,  $T_c = 252.8^\circ\text{C}$ , and  $\epsilon_r = 1820$ ). By co-firing experiments with Cu electrodes and piezoelectric ceramic materials, they found no appreciable diffusion between the two materials, and proved the viability of employing Cu electrodes for multilayer actuators. Zhang et al.<sup>17</sup> investigated the effect of CuO and LiBiO<sub>2</sub> co-doping on the sintering temperature of Pb(Ni<sub>1/3</sub>Nb<sub>2/3</sub>)O<sub>3</sub>–Pb(Zr<sub>0.41</sub>Ti<sub>0.59</sub>)O<sub>3</sub> (PNN–PZT) piezoelectric ceramics, and successfully lowered the sintering temperature of PNN–PZT to 960°C by using CuO and LiBiO<sub>2</sub> co-doping. The piezoelectric properties of PZT ceramics, which provide a reference for the selection of materials for multilayer piezoelectric devices, were also flexibly tuned by adjusting the amount of LiBiO<sub>2</sub> doping. When PNN–PZT ceramics with 0.2 wt.% CuO and 1.0 wt.% LiBiO<sub>2</sub> have good electrical properties ( $d_{33} = 608$  pC/N,  $T_c = 191.6^\circ\text{C}$ ,  $k_p = 0.65$ , and  $\epsilon_r = 3843$ ).

LiBiO<sub>2</sub> can lower the sintering temperature of PZT by forming a liquid phase. However, Li<sup>+</sup> in LiBiO<sub>2</sub> will replace Pb<sup>2+</sup> at the A-position or Ti<sup>4+</sup> at the B-position in the perovskite structure during sintering, creating oxygen vacancies to balance the charge. The presence of oxygen vacancies causes a "pegging effect" on the steering of the domains, preventing polarization flipping, which makes it difficult for the material polarization.<sup>18</sup> In addition, Bi<sub>2</sub>O<sub>3</sub> has a relatively low melting point and can form a liquid phase during sintering, which prevents the formation of oxygen vacancies. In this paper, PZT-5H piezoelectric ceramics with excellent electrical properties were successfully prepared with Bi<sub>2</sub>O<sub>3</sub> as the sintering aid, and densified at 850°C. The effects of the doping amount of Bi<sub>2</sub>O<sub>3</sub> on the sintering properties, microstructure, and electrical properties of PZT-5H piezoelectric ceramics were also investigated. Additionally, by assessing the electrical properties and microstructure, it was shown that multilayer piezoelectric ceramic actuators with this material can be used in real-world applications.

## Experimental

### Ceramic Powder and Monolayer Sample Preparation

Piezoelectric ceramics were prepared using the conventional solid-state sintering method. The composition of the PZT-5H ceramics used was 0.38Pb(Mg<sub>1/3</sub>Nb<sub>2/3</sub>)O<sub>3</sub>–0.62Pb(Zr<sub>0.4</sub>Ti<sub>0.6</sub>)O<sub>3</sub> + 0.4wt.%CuO + xwt.%Bi<sub>2</sub>O<sub>3</sub>.

PbO (98%), MgO (99.8%), Nb<sub>2</sub>O<sub>5</sub> (99.99%), ZrO<sub>2</sub> (99.5%), TiO<sub>2</sub> (99.8%), and H<sub>2</sub>O zirconia balls were weighed and placed in a grinding jar and finely ground for 24 h. The mixed powder was calcined at 950°C for 4 h after drying. The calcined ceramic powder, CuO (99%), and Bi<sub>2</sub>O<sub>3</sub> (99%), were then placed in a grinding jar and finely ground for 12 h. The secondary finely ground powder was granulated with a 7% mass fraction of PVA solution and pressed at 4-MPa pressure into ceramic flakes with a diameter of 17 mm and a thickness of about 1.0 mm. The binder was removed from the raw ceramic at 650°C, and sintering was completed at 850°C. The sintered ceramic samples were polished, coated with silver paste, and calcined at 650°C for 0.5 h. The calcined ceramic pieces were polarized in silicone oil at 120°C with a polarization field strength of 3 kV/mm and a polarization time of 30 min. The ceramic samples were finally cleaned and aged for 24 h before being used for electrical characterization.

### Piezoelectric Actuator Preparation

PZT-5H + 0.4 wt.% CuO + 0.9 wt.% Bi<sub>2</sub>O<sub>3</sub> as the experimental formulation, a binary azeotrope of butanone (30 wt.%) and anhydrous ethanol (70 wt.%) as the solvent, polyvinyl butyral (PVB) as the binder, dibutyl phthalate (DBP) as the plasticizer and triethyl phosphate as the dispersant. The specific preparation process is shown in Fig. 1. PZT powder, absolute ethanol, butanone, and a dispersant were mixed for initial ball milling. After 24 h of ball milling, the binder, PVB, and plasticizer, DBP, were added for secondary ball milling to obtain PZT tape casting slurry, and finally formed PZT thick film material on the tape-casting machine. The silver paste was printed on the PZT thick film and the film laminated into a specific structure. The actuator blanks were heated at a rate of 1°C/min to 550°C to remove the organic binder and sintered at 850°C for 2 h to obtain the desired actuator sample.

### Testing and Characterization

The bulk density of the ceramic samples was determined according to the Archimedean drainage method. The microstructure of the ceramic sample sections was observed with a field-emission scanning electron microscopy (FE-SEM; S-4800; Hitachi, Tokyo, Japan). The crystal structure of the ceramic specimens was characterized by x-ray diffraction (XRD; D8 Advance; Bruker, Germany). The piezoelectric coefficients were measured by a quasi-static  $d_{33}$  tester (ZJ-4AN; Institute of Acoustics, Chinese Academy of Sciences). The mechanical quality factor, electromechanical coupling coefficient, the relative dielectric constant, and dielectric loss were measured by an LCR impedance analyzer (1260A + 1296A; Solartronanalytical, UK). The sample's

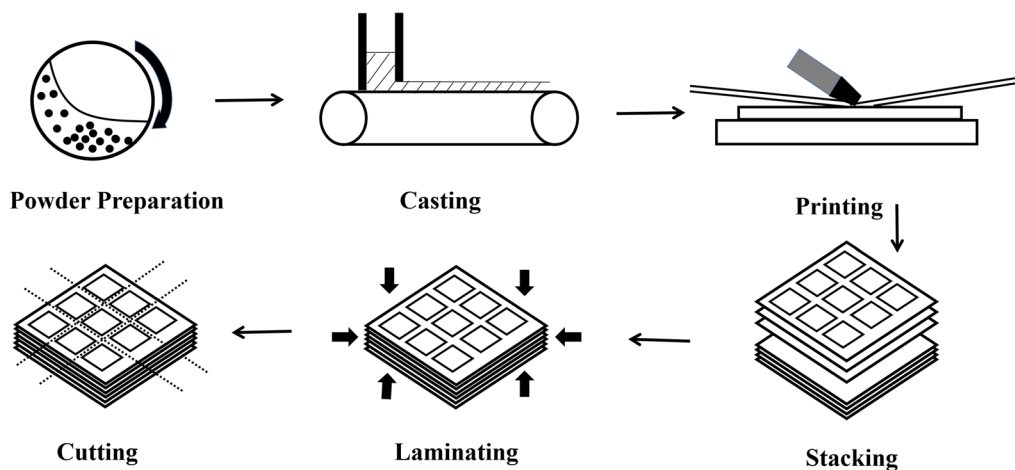


Fig. 1 Multi-layer piezoelectric ceramic actuator preparation process.

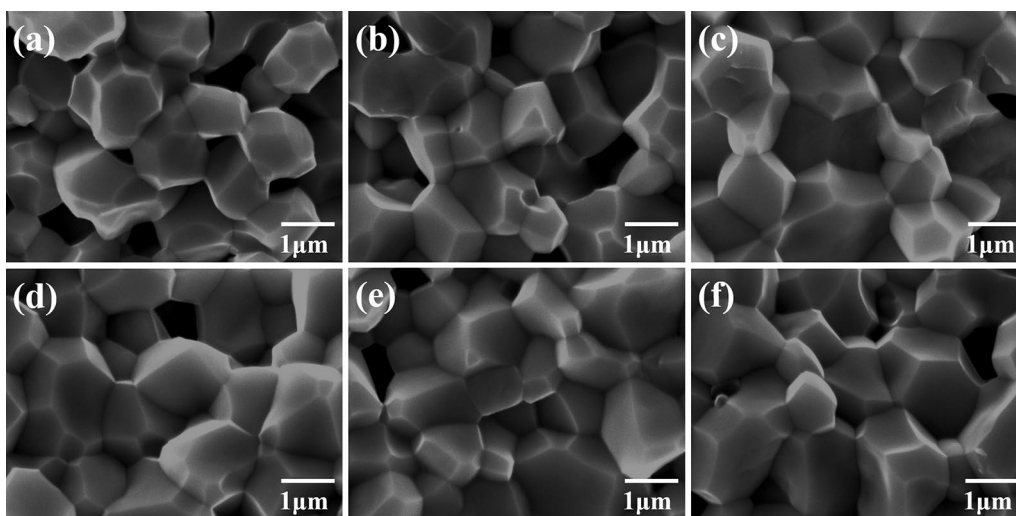


Fig. 2 Cross-section SEM images of different  $\text{Bi}_2\text{O}_3$  doping samples: (a) 0.7 wt.%, (b) 0.8 wt.%, (c) 0.9 wt.%, (d) 1.0 wt.%, (e) 1.1 wt.%, (f) 1.2 wt.%.

Curie temperature ( $T_c$ ) was determined using a broadband dielectric impedance measurement system (Concept 80; Novocontrol, Germany). The ferroelectric properties of the samples were measured using a ferroelectric analyzer (RTI-Multiferroic; Radiant, USA).

## Results and Discussion

### Physical Properties and Microstructure

Figure 2 shows cross-sectional SEM images of samples sintered at  $850^\circ\text{C}$  with different  $\text{Bi}_2\text{O}_3$  doping levels. No second phase or segregation was observed in the piezoelectric ceramics, and all the specimens were fractured in the

form of intergranular fracture. When doping 0.7 wt.% and 0.8 wt.% sintering additives of  $\text{Bi}_2\text{O}_3$ , the grain development was poor, the grain size distribution was not uniform, and there were many pores in the sample. This phenomenon was because the liquid phase produced by  $\text{Bi}_2\text{O}_3$  was too little to adequately wet the grain surface, resulting in poor grain development. As shown in Fig. 3, with the increase of  $\text{Bi}_2\text{O}_3$  doping, the densities of the ceramics increased, the grain size distribution was uniform, the grain boundaries were clear, and there were few pores in the samples. This indicates that the appropriate amount of liquid phase can fully infiltrate the ceramic particles during the sintering process, which effectively enhances the sintering ability of the PZT-5H ceramics and promotes grain growth.<sup>19</sup> With the further increase of the  $\text{Bi}_2\text{O}_3$  content, it was found that the

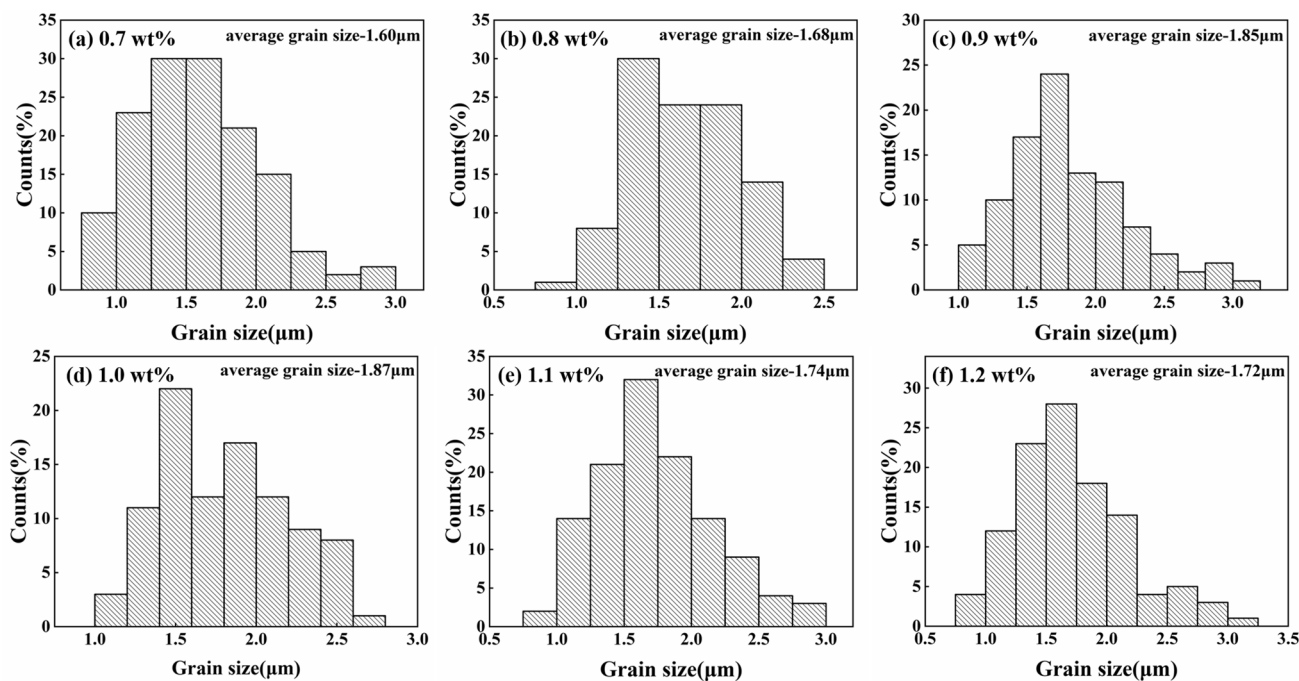


Fig. 3 Grain size distribution and average grain size for the piezoceramics with different Bi<sub>2</sub>O<sub>3</sub> amounts.

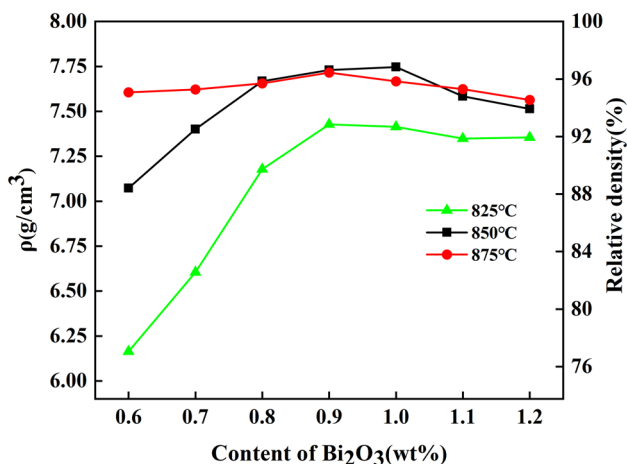


Fig. 4 Schematic of the variation of the density of PZT-5H ceramics with the change of Bi<sub>2</sub>O<sub>3</sub> doping at different sintering temperatures.

pores of the samples started to increase again. This is due to the addition of an excess of Bi<sub>2</sub>O<sub>3</sub>, resulting in an excess of liquid phase. It collects at the grain boundaries and not only inhibits the mass transfer process, causing the grain to stop growing, but also discourages the exclusion of pores, resulting in a decrease in the density of the ceramic.<sup>20,21</sup>

Figure 4 shows the density of PZT-5H ceramics at different sintering temperatures as a function of sintering temperature. It can be seen that the density of the samples showed a trend of increasing and then stabilized with the increase of Bi<sub>2</sub>O<sub>3</sub> doping at the same sintering temperature.

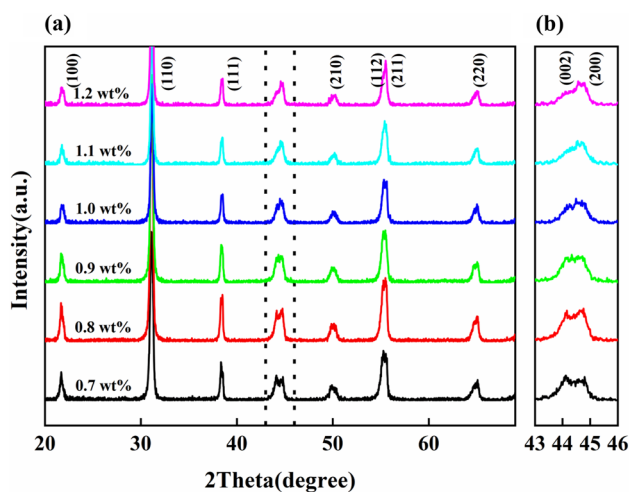
When doping with 0.9 wt.% sintering additives of Bi<sub>2</sub>O<sub>3</sub>, the maximum density was obtained. When too little Bi<sub>2</sub>O<sub>3</sub> (melting point: 825°C) is added, the resulting liquid phase is not sufficient to promote the movement of grain boundaries, but instead impurities are formed at the grain boundaries, reducing the density of the ceramic. The liquid phase formed by adding the right amount of Bi<sub>2</sub>O<sub>3</sub> can promote contact between grain interfaces, which is conducive to grain growth and the discharge of pores, accelerating the densification of the ceramic.<sup>20</sup> However, when the doping of Bi<sub>2</sub>O<sub>3</sub> is higher than 0.9 wt.%, an excess liquid phase is formed, which inhibits the growth of ceramic grains, increases the porosity, and leads to a decrease in ceramic density.<sup>22</sup>

Figure 5a shows the XRD patterns of PZT-5H ceramics doped with different levels of Bi<sub>2</sub>O<sub>3</sub>. All samples show a pure perovskite structure without any detectable secondary phase, indicating that Bi<sub>2</sub>O<sub>3</sub> can ultimately form a solid solution structure with PZT-5H.<sup>12,23</sup> For the PZT system, there are two different phase structures, the rhombohedral and the tetragonal, as the components of the PZT change. According to crystallographic knowledge, the (200) and the (002) crystal planes are equivalent to the tetragonal phase. Therefore, split into two peaks at this angle: the peak (200) at the high angle and the peak (002) at the low angle, with an intensity ratio of roughly 2:1. For the rhombohedral phase, the peaks (200), (020), and (002) are all equivalent, resulting in only a single peak. Figure 5b shows an enlarged view of the characteristic peak, and, as can be seen, as the amount of Bi<sub>2</sub>O<sub>3</sub> added decreases (less than 1.0 wt.%), a

more prominent broad peak appears near  $45^\circ$ , mainly due to the presence of a rhombohedral phase in the tetragonal structure. The component is in a rhombohedral–tetragonal phase coexistence structure called the morphotropic phase boundary (MPB). With the increase of  $\text{Bi}_2\text{O}_3$  doping content ( $> 1.0$  wt.%), the characteristic peak splitting of PZT gradually decreases, indicating that the content of the rhombohedral phase gradually increases and that the content of the tetragonal phase decreases.

## Electrical Properties

The trend in relative permittivity ( $\epsilon_r$ ) with  $\text{Bi}_2\text{O}_3$  doping is the same as for  $d_{33}$  and  $k_p$ , as shown in Fig. 6. The appropriate amount of  $\text{Bi}_2\text{O}_3$  produces a liquid phase during the sintering process. The liquid phase can effectively promote sintering, resulting in uniform grain growth and larger grain



**Fig. 5** XRD patterns of PZT-5H +  $x$  wt.% ( $\text{Bi}_2\text{O}_3$ ) ceramics with  $0.7 \leq x \leq 1.2$  sintered at  $850^\circ\text{C}$ : (a)  $2\theta$  in the range of  $20\text{--}80^\circ$ , (b)  $2\theta$  in the range of  $43\text{--}46^\circ$ .

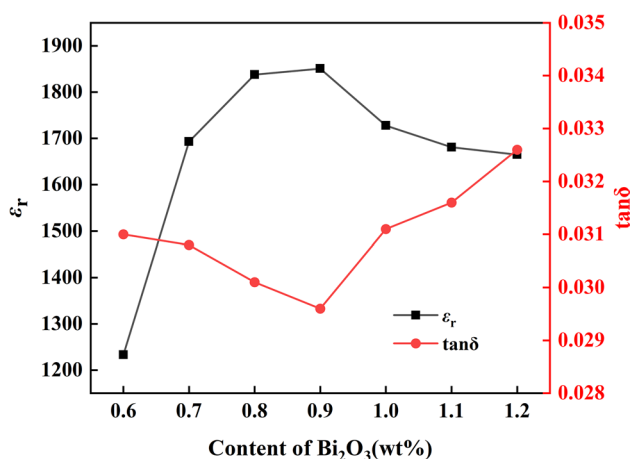


**Fig. 6**  $\epsilon_r$ ,  $\tan\delta$  properties of samples with different amounts of  $\text{Bi}_2\text{O}_3$ .

size, and reducing the number of pores, thus reducing the grain boundary area and increasing the relative permittivity. When the doping was below 0.8 wt.%, the amount of liquid phase produced in the sintering process was insufficient, the grain growth was inadequate, the pore content was higher, and the area occupied by the grain boundary was large, so its relative permittivity ( $\epsilon_r$ ) was very low. When an excessive amount of  $\text{Bi}_2\text{O}_3$  was added, the number of abnormally nucleated grains increases during sintering. The liquid film also blocks the mass transfer, so the sintered ceramic grains are not uniform in size, the density decreases, and the relative permittivity decreases.<sup>24</sup>

It can be seen in Fig. 7 that the piezoelectric constant  $d_{33}$  of the samples increased substantially with increasing the  $\text{Bi}_2\text{O}_3$  content when the  $\text{Bi}_2\text{O}_3$  doping was below 0.8 wt.%; when the  $\text{Bi}_2\text{O}_3$  doping continued to increase, the  $d_{33}$  of the ceramic samples gradually decreased. The low  $d_{33}$  at low  $\text{Bi}_2\text{O}_3$  doping is because the smaller liquid phase does not sufficiently infiltrate the grain boundaries, resulting in low density and high porosity. At the same time, the stress around the pores prevents grain growth and domain movement, resulting in poor piezoelectric properties of the sample.<sup>25</sup> When the doping level is too high, the large amount of liquid phase affects the densification process of the ceramic and therefore leads to a decrease in  $d_{33}$ .<sup>15</sup>

The electromechanical coupling factor ( $k_p$ ) value of the ceramics increases rapidly with the increase of  $\text{Bi}_2\text{O}_3$  content when the doping amount is less than 0.9 wt.%. The maximum value of  $k_p$  was achieved when the doping amount was 0.9 wt.%, after which the  $k_p$  value decreased with the increase of  $\text{Bi}_2\text{O}_3$  content. This phenomenon was because, when the doping amount is 0.9 wt.%, the ceramics have good grain growth, uniform grain size, and fewer defects and pores. At the same time, the presence of a large number of dense grain boundaries is conducive to increasing  $k_p$ . When the doping amount continues to increase,  $\text{Bi}^{3+}$  precipitates

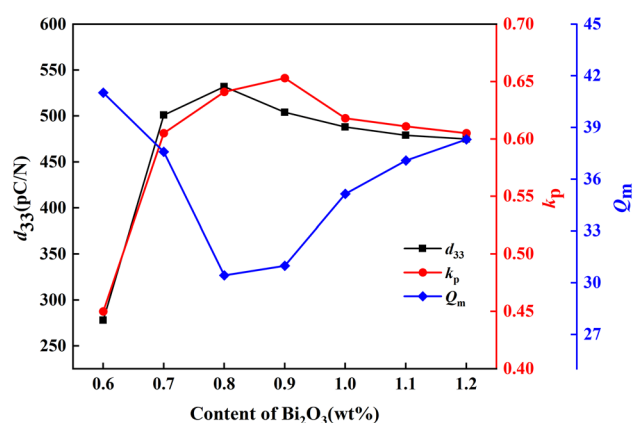


**Fig. 7**  $d_{33}$ ,  $k_p$ ,  $Q_m$  properties of samples with different amounts of  $\text{Bi}_2\text{O}_3$ .

on the grain boundaries due to saturation and prevents average grain growth, resulting in poor dense ceramics and reduced  $k_p$ .<sup>15,25</sup> The variation of the mechanical quality factor ( $Q_m$ ) with Bi<sub>2</sub>O<sub>3</sub> doping is the opposite of the interpretation of  $k_p$  with Bi<sub>2</sub>O<sub>3</sub> doping.

The trend of the  $\tan\delta$  is opposite to that of  $\epsilon_r$ . The  $\tan\delta$  decreases and then increases with increasing Bi<sub>2</sub>O<sub>3</sub> content. The  $\tan\delta$  are caused by friction between the domain walls and the defects, between the domain walls and the crystals, and between the domain walls. The  $\tan\delta$  were relatively low when less energy was consumed in the movement and spontaneous polarization of the electric domains. When the doping amount was 0.9 wt.%, the distribution of grains is uniform, the bond between grains is tight, the density is high, and the defects are few. This facilitates the movement of the domain walls and the orientation of spontaneous polarization, so that the dielectric loss of the sample is reduced.<sup>26</sup>

Figure 8a shows the measurement results of the  $P$ - $E$  curve with a variation in the amount of Bi<sub>2</sub>O<sub>3</sub> (test frequency 1 Hz). As shown, all the samples have typical hysteresis loops. The introduction of Bi<sub>2</sub>O<sub>3</sub> can improve the piezoelectric and ferroelectric properties to some extent. At a doping level of 0.9 wt.%, the ceramics have a maximum residual polarization intensity of 36.659  $\mu\text{C}/\text{cm}^2$ . When doped with the right amount of Bi<sub>2</sub>O<sub>3</sub>, the sample had tight intergranular bonding, a high density, and few defects. This facilitates the movement of the domain walls, so the residual polarization strength of the ceramic increases with the increase of the doping amount. However, when the Bi<sub>2</sub>O<sub>3</sub> content was too high, the ferroelectricity of the ceramic material decreases due to the presence of non-ferroelectric phase impurities.<sup>27,28</sup>

Figure 9 shows the relative permittivity of the PZT-5H piezoelectric ceramics as a function of temperature during the temperature rise from room temperature to 300°C at a test frequency of 1 kHz. As shown in Fig. 8, the dielectric

properties of the PZT-5H piezoelectric ceramics exhibit the characteristics of a relaxation material, with the phase transition occurring over a wide temperature range. The phase transition temperature (Curie temperature,  $T_c$ ) of the cubic and tetragonal phases of PZT-5H piezoelectric ceramics with different doping levels was about 230°C, and the peak of the dielectric constant decreased with increasing doping levels. Some researchers have used the "brick-wall" model to explain the relationship between dielectric peak broadening and grain size.<sup>29</sup> The total dielectric constant of the ceramics can be divided into two parts, the grain dielectric constant and the grain boundary dielectric constant. These two components are arranged electrically in series, and the proportion of each is determined by their volume fraction. The dielectric constant peaks when the isolated grain phase undergoes a curie phase transition from low to high temperature. In contrast, the continuous grain boundary phase maintained a lower dielectric constant value, which diluted the total dielectric constant, resulting in a lower dielectric peak. As the grain size decreased, the volume fraction of the grain boundaries increased, and the dilution effect became more pronounced, resulting in a more significant reduction in the dielectric peak.

### Microstructure and Electrical Properties of Multilayer Piezoelectric Ceramic Actuators

Figure 10 shows the SEM images of the cross-section of the multilayer actuator sintered at 850°C. As shown in Fig. 10a-c, the boundary between the ceramic layer and the inner electrode layer is obvious, the thickness between the layers is relatively uniform, and the whole is rather neat, while the grain size in the ceramic coating is uniform, the microstructure is relatively dense. Figure 10e-h shows the corresponding elemental mappings of the

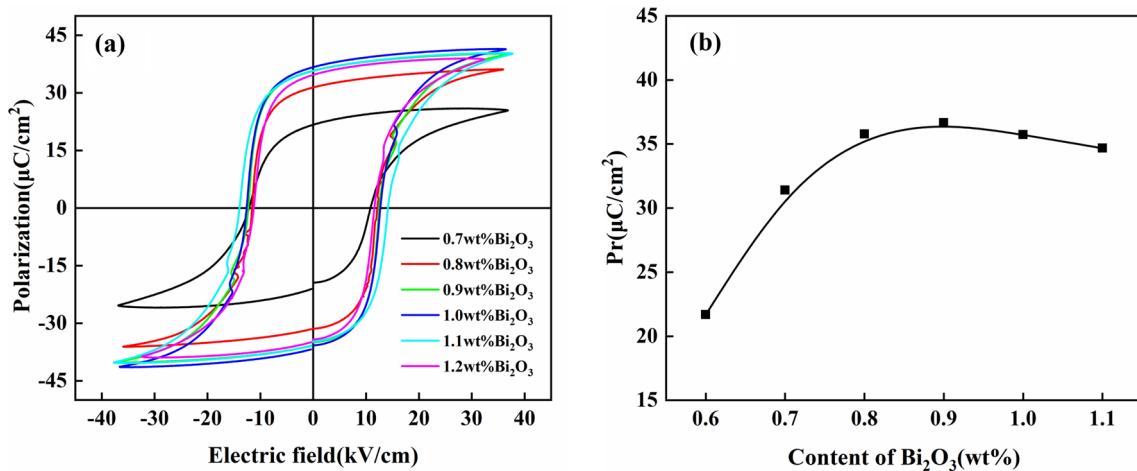
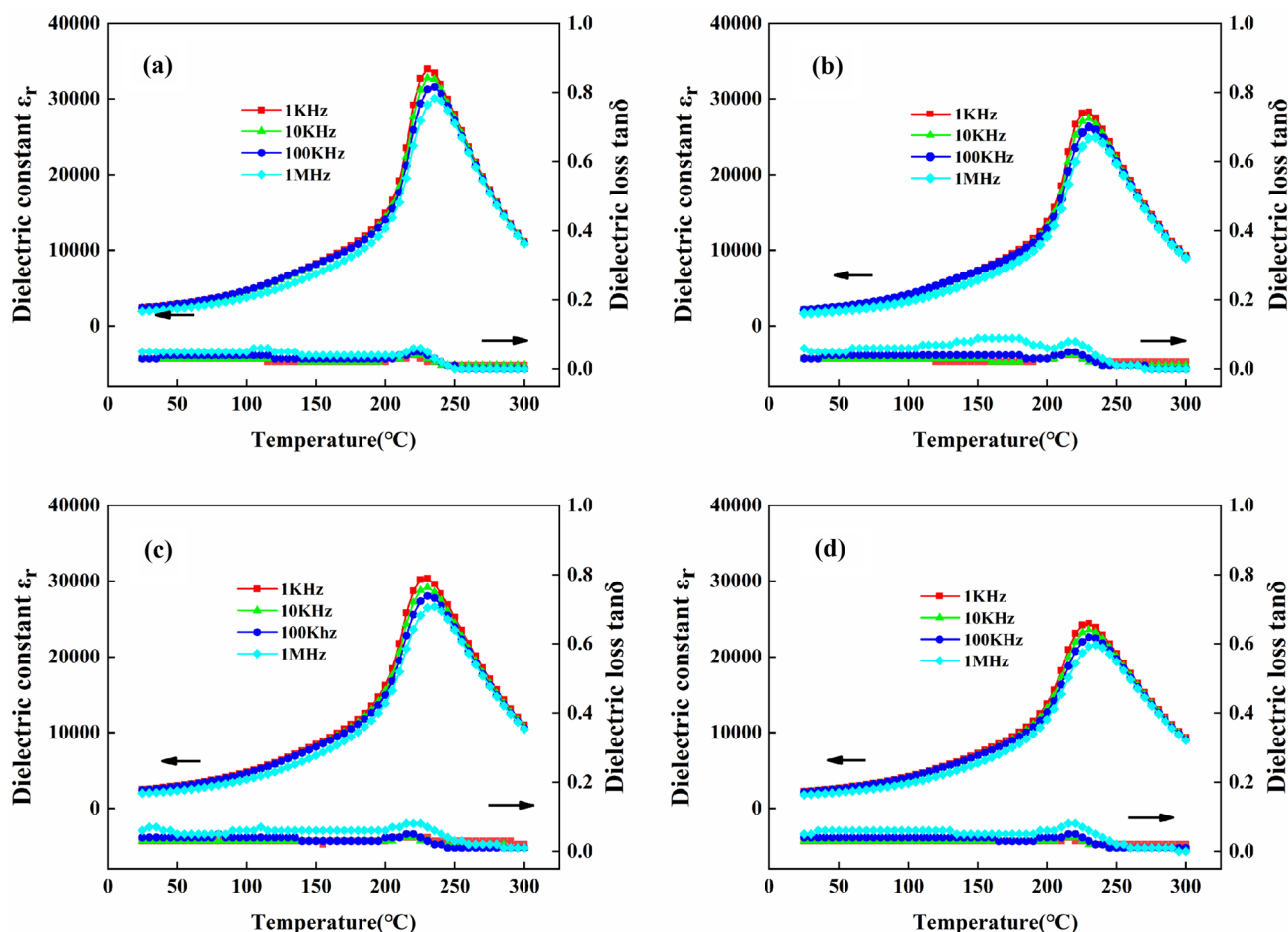


Fig. 8 (a)  $P$ - $E$  hysteresis loops, (b)  $P_r$  of PZT-5H +  $x$  wt.% (Bi<sub>2</sub>O<sub>3</sub>) ceramics sintered at 850°C with  $x$  from 0.7 to 1.2.



**Fig. 9** Dielectric temperature spectra of samples with different amounts of  $\text{Bi}_2\text{O}_3$ : (a) 0.7 wt.%, (b) 0.8 wt.%, (c) 0.9 wt.%, (d) 1.0 wt.%.

laminated device. The Ag elements were concentrated in the electrode layers and did not diffuse significantly into the ceramic coating. The results showed that the laminar actuator is well structured and has good conductivity for functional components.

Figure 11 shows the monopole  $S$ – $E$  curves for a multilayer actuator prepared using the tape-casting process versus a single layer actuator prepared using the conventional method. By testing the actuator drive voltage versus strain, the multilayer actuator achieved a displacement of  $2.18 \mu\text{m}$  and a strain of 0.109% at 600 V. In comparison, the single-layer actuator was only able to achieve displacement and strain of  $0.25 \mu\text{m}$  and 0.021% at 600 V. The results show that the laminated actuator can produce large displacements at low drive voltages, confirming the possibility of using the material in multilayer laminated piezoelectric ceramic components.

## Conclusions

The effects of  $\text{Bi}_2\text{O}_3$  on the microstructure, phase composition, and electrical properties of piezoelectric ceramics were investigated, as were the application possibilities to multilayer piezoelectric ceramic components using PZT-5H piezoelectric ceramic powder as the object of study. When the doping amount of  $\text{Bi}_2\text{O}_3$  was less than 1.0 wt.%, the crystal structure of PZT-5H piezoelectric ceramics lay at the morphotropic phase boundary (MPB), and, when the doping amount of  $\text{Bi}_2\text{O}_3$  was further increased, the crystal structure of piezoelectric ceramics transformed to the rhombohedral phase.  $\text{Bi}_2\text{O}_3$  could lower the sintering temperature of PZT-5H piezoelectric ceramics to  $850^\circ\text{C}$ . When doped with 0.9 wt.%  $\text{Bi}_2\text{O}_2$ , PZT-5H piezoelectric ceramics could obtain the best overall performance:  $d_{33} = 504\text{pC/N}$ ,  $\epsilon_r = 1851$ ,  $k_p = 0.653$ ,  $Q_m = 30.983$ , and

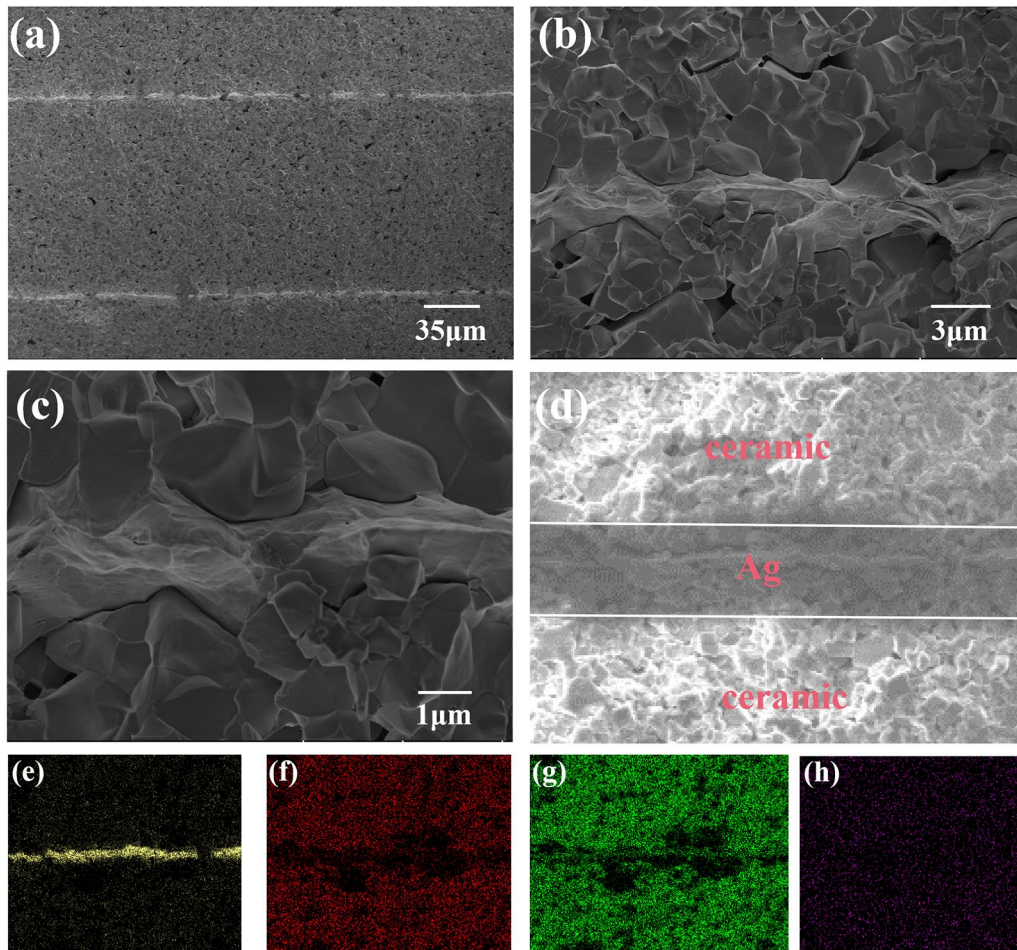


**Fig. 10** (a–d) Cross-sectional SEM images of the laminated device and the corresponding elemental mappings of (e) Ag, (f) Ti, (g) Zr, and (h) Pb in the same region of (d).

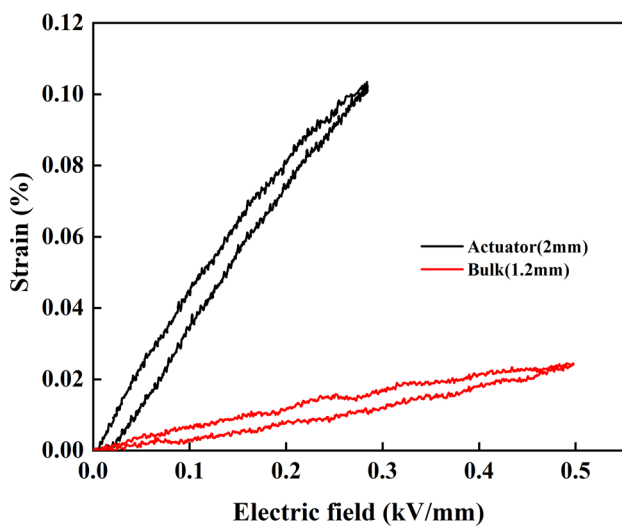


**Fig. 11** Single pole *S–E* curves for multilayer and single layer actuators.

$\tan \delta = 0.0296$ . Co-firing experiments of PZT-5H ceramics with silver electrodes and performance tests of multilayer actuators have shown that low-temperature-sintered PZT-5H ceramics could be used to prepare multilayer piezoelectric ceramic components. Multilayer actuators were more advantageous in low driving voltage applications than conventional actuators. When a 600-V drive voltage was applied, the strain value of the laminated piezoelectric actuator reached 0.109%.

**Acknowledgments** This work was supported by the National Natural Science Foundation of China (Grant Nos. U1806221, 51672198, 51572204 and 51072146), Innovation and Development Project of Zibo City (2017CX01A022), Instruction & Development Project for National Funding Innovation Demonstration Zone of Shandong Province (2018ZCQZB01, 2019ZCQZB03), Central Guiding Local Science and Technology Development Special Funds (Grant Nos. 2060503), and Key Research & Design Program of Shandong Province (2019GGX102011).



**Conflict of interest** No conflict of interest exists in the submission of this manuscript, and manuscript is approved by all authors for publication.

## References

1. Y. Luo, T. Pu, S. Fan, H. Liu, and J. Zhu, Enhanced piezoelectric properties in low-temperature sintering PZN–PZT ceramics by adjusting Zr/Ti ratio. *J. Adv. Dielectr.* 12, 6 (2022).
2. S.W. Kim, J.J. Yong, and H.C. Lee, Effects of the mixing method and sintering temperature on the characteristics of PZNN–PZT piezoelectric ceramic materials. *J. Korean Powder Metall. Inst.* 25, 487 (2018).
3. X.Y. Gao, X.D. Xin, J.G. Wu, Z.Q. Chu, and S.X. Dong, A multi-layered-cylindrical piezoelectric shear actuator operating in shear ( $d_{15}$ ) mode. *App. Phys. Lett.* 112, 152902 (2018).
4. X.Y. Gao, Z.M. Li, J.G. Wu, X.D. Xin, X.Y. Shen, X.T. Yuan, J.K. Yang, Z.Q. Chu, and S.X. Dong, A piezoelectric and electromagnetic dual mechanism multimodal linear actuator for generating macro- and nanomotion. *Research* 2019, 8232097 (2019).
5. R. Nie, Q. Zhang, Y. Yue, H. Liu, Y. Chen, Q. Chen, J. Zhu, P. Yu, and D. Xiao, Phase structure–electrical property relationships in  $\text{Pb}(\text{Ni}_{1/3}\text{Nb}_{2/3})\text{O}_3\text{--Pb}(\text{Zr}, \text{Ti})\text{O}_3$ -based ceramics. *J. Appl. Phys.* 119, 124111 (2016).
6. K. Wen, J.H. Qiu, H.L. Ji, K.J. Zhu, J.S. Liu, J. Wang, J.Z. Du, and F.L. Zhu, Investigation of phase diagram and electrical properties of  $x\text{Pb}(\text{Mg}_{1/3}\text{Nb}_{2/3})\text{O}_3\text{--}(1-x)\text{Pb}(\text{Zr}_{0.4}\text{Ti}_{0.6})\text{O}_3$  ceramics. *J. Mater. Sci. Mater. Electron.* 25, 3003 (2014).
7. S.Y. Kweon, K.S. Lee, Y.M. Park, and M.S. Yoon, Low-temperature sintering of  $(1-x)\text{Pb}(\text{Zr}_{0.53}\text{Ti}_{0.47})\text{O}_3\text{--}x\text{BiYO}_3$  ceramics with nano-powder for piezo-speaker. *Jpn. J. Appl. Phys.* 58, 9 (2019).
8. W. Zhang and R.E. Eitel, Sintering behavior, properties, and applications of co-fired piezoelectric/low temperature co-fired ceramic (PZT–SKN/LTCC) multilayer ceramics. *Int. J. Appl. Ceram. Technol.* 2, 354 (2013).
9. H. Chen, T. Pu, Y. Luo, S. Fan, Q. Chen, H. Liu, and J. Zhu, Enhancement of piezoelectric properties in low-temperature sintering PZN–PZT ceramics by  $\text{Sr}^{2+}$  substitution. *J. Electron. Mater.* 51, 1261 (2022).
10. H. Chen, T. Pu, S. Fan, H. Liu, J. Zhu, and Q. Chen, Enhanced electrical properties in low-temperature sintering PNN–PMW–PZT ceramics by  $\text{Yb}_2\text{O}_3$  doping. *Mater. Res. Bull.* 146, 111576 (2022).
11. C.H. Nam, H.Y. Park, I.T. Seo, J.H. Choi, S. Nahm, and H.G. Lee, Effect of CuO on the sintering temperature and piezoelectric properties of  $\text{MnO}_2$ -doped  $0.75\text{Pb}(\text{Zr}_{0.47}\text{Ti}_{0.53})\text{O}_3\text{--}0.25\text{Pb}(\text{Zn}_{1/3}\text{Nb}_{2/3})\text{O}_3$  ceramics. *J. Alloys Compd.* 509, 3686 (2011).
12. Y. Jeong, J. Yoo, S. Lee, and J. Hong, Piezoelectric characteristics of low temperature sintering  $\text{Pb}(\text{Mn}_{1/3}\text{Nb}_{2/3})\text{O}_3\text{--Pb}(\text{Ni}_{1/3}\text{Nb}_{2/3})\text{O}_3\text{--Pb}(\text{Zr}_{0.50}\text{Ti}_{0.50})\text{O}_3$  according to the addition of CuO and  $\text{Fe}_2\text{O}_3$ . *Sens. Actuators A Phys.* 135, 215 (2007).
13. Y.D. Hou, M.K. Zhu, H. Wang, B. Wang, H. Yan, and C.S. Tian, Effects of CuO addition on the structure and electrical properties of low temperature sintered  $\text{Pb}((\text{Zn}_{1/3}\text{Nb}_{2/3})_{(0.20)}(\text{Zr}_{0.50}\text{Ti}_{0.50})_{(0.80)})\text{O}_3$  ceramics. *Mater. Sci. Eng. B Solid State Mater. Adv. Technol.* 110, 27 (2004).
14. C.W. Ahn, H.C. Song, S. Nahm, and S. Priya, Effect of ZnO and CuO on the sintering temperature and piezoelectric properties of a hard piezoelectric ceramic. *J. Am. Ceram. Soc.* 89, 921 (2006).
15. J.Q. Yi, S.L. Jiang, S.S. Liu, L. Zhang, and J.G. He, Effects of  $\text{LiBiO}_2$  addition on the microstructure and piezoelectric properties of CuO-doped PNN–PZT ceramics. *Phys. Status Solidi A Appl. Mater.* 211, 2552 (2014).
16. S.C. Hong, S.Y. Kim, D.H. Yeo, H.S. Shin, Z.H. Park, and S. Nahm, Effect of  $\text{LiBiO}_2$  on low-temperature sintering of PZT–PZNN ceramics. *J. Korean Ceram. Soc.* 59, 638 (2022).
17. J. Zhang, Y.S. Zhang, Z.M. Yan, A.J. Wang, P. Jiang, and M. Zhong, Fabrication and performance of PNN–PZT piezoelectric ceramics obtained by low-temperature sintering. *Sci. Eng. Compos. Mater.* 27, 359 (2020).
18. L. Shi, P.L. Wu, L.T. Yu, Y. Zhao, Z. Li, W.Y. Zhao, Z. Wang, Y.Z. Peng, W.J. Hua, J. Wang, R.X. Song, and W.D. Fei, Enhanced piezoelectric properties and phase transition in PZT ceramics induced by  $\text{Li}^+\text{--Sm}^{3+}$  ionic pairs. *Ceram. Int.* 48, 10024 (2022).
19. D.L. Corker, R.W. Whatmore, E. Ringgaard, and W.W. Wolny, Liquid-phase sintering of PZT ceramics. *J. Eur. Ceram. Soc.* 20, 2039 (2000).
20. T.C. Zhou, H.W. Zhang, L.J. Jia, J. Li, Y.L. Liao, L.C. Jin, and H. Su, Grain growth, densification, and gyromagnetic properties of  $\text{LiZnTi}$  ferrites with  $\text{H}_3\text{BO}_3\text{--Bi}_2\text{O}_3\text{--SiO}_2\text{--ZnO}$  glass addition. *J. Appl. Phys.* 115, 3 (2014).
21. Y.C. Zhang, W.N. Ye, Z.Z. Yang, C.J. Lu, and L.H. Xia, Effect of excess Pb on formation of perovskite-type  $0.67\text{Pb}(\text{Mg}_{1/3}\text{Nb}_{2/3})\text{O}_3\text{--}0.33\text{PbTiO}_3$  powders synthesized through a sol–gel process. *J. Mater. Sci. Mater. Electron.* 22, 91 (2011).
22. D. Saha, A. Sen, and H.S. Maiti, The role of dilatancy on expansion during early stage liquid phase sintering of lead magnesium niobate. *Ceram. Int.* 27, 51 (2001).
23. Q. Zhang, Y. Yue, R. Nie, H. Liu, Q. Chen, P. Yu, J.G. Zhu, and D.Q. Xiao, Achieving both high  $d_{33}$  and high  $T_c$  in low-temperature sintering  $\text{Pb}(\text{Ni}_{1/3}\text{Nb}_{2/3})\text{O}_3\text{--Pb}(\text{Mg}_{1/2}\text{W}_{1/2})\text{O}_3\text{--Pb}(\text{Zr}_{0.5}\text{Ti}_{0.5})\text{O}_3$  ceramics using  $\text{Li}_2\text{CO}_3$ . *Mater. Res. Bull.* 85, 96 (2017).
24. Y.K. Zeng, F. Yao, G.Z. Zhang, S.S. Liu, S.L. Jiang, Y. Yu, J.G. He, L. Zhang, and J.Q. Yi, Effects of  $\text{Bi}_2\text{O}_3\text{--Li}_2\text{CO}_3$  additions on dielectric and pyroelectric properties of Mn doped  $\text{Pb}(\text{Zr}_{0.9}\text{Ti}_{0.1})\text{O}_3$  thick films. *Ceram. Int.* 39, 3709 (2013).
25. H. Zhang, J. Shen, J. Tian, J. Zhou, and W. Chen, Elastic, dielectric and piezoelectric properties of  $\text{Fe}_2\text{O}_3$  doped PMnS–PZN–PZT ceramics. *Ferroelectrics* 491, 15 (2016).
26. B. Shao, J.H. Qiu, K.J. Zhu, Y. Cao, and H.L. Ji, Effect of CuO on dielectric and piezoelectric properties of  $(\text{K}_{0.4425}\text{Na}_{0.52}\text{Li}_{0.0375})(\text{Nb}_{0.87}\text{Ta}_{0.06}\text{Sb}_{0.07})\text{O}_3$  ceramics. *J. Alloys Compd.* 515, 128 (2012).
27. Y.R. Wang, and S.F. Wang, Liquid phase sintering of NiCuZn ferrite and its magnetic properties. *Int. J. Inorg. Mater.* 3, 1189 (2001).
28. S. Li, J. Fu, and R.Z. Zuo, Middle-low temperature sintering and piezoelectric properties of CuO and  $\text{Bi}_2\text{O}_3$  doped PMS–PZT based ceramics for ultrasonic motors. *Ceram. Int.* 47, 20117 (2021).
29. A.V. Polotai, A.V. Ragulya, and C.A. Randall, Preparation and size effect in pure nanocrystalline barium titanate ceramics. *Ferroelectrics* 288, 93 (2003).

**Publisher's Note** Springer Nature remains neutral with regard to jurisdictional claims in published maps and institutional affiliations.

Springer Nature or its licensor (e.g. a society or other partner) holds exclusive rights to this article under a publishing agreement with the author(s) or other rightsholder(s); author self-archiving of the accepted manuscript version of this article is solely governed by the terms of such publishing agreement and applicable law.